Int J CARS (2013) 8 (Suppl 1):S183–S187
DOI 10.1007/s11548-013-0867-x

C-arm angle measurement with accelerometer for brachytherapy—an accuracy study

T. Wolff[1], A. Lasso[2], M. Eblenkamp[1], E. Wintermantel[1], G. Fichtinger[2]
[1]Technical University Munich, Faculty of Mechanical Engineering, Munich, Germany
[2]Queen's University, School of Computing, Kingston, ON, Canada

Keywords Accelerometer · C-Arm · Angle Measurement · Accuracy Study

Purpose
Measure the rotation of a C-arm fluoroscopy with three-axis accelerometer for prostate brachytherapy implantation.
Methods
Basic idea is to use the three-axis accelerometer as a tilt sensor at static positions, which has not been done on a C-arm before. Following on the work of Grzeda et al. [1], we use an accelerometer with higher resolution on a full-size clinical C-arm. We used an optical tracking system to verify the measured C-arm angles. In addition we calibrated the C-arm as in [2] and [3] and compared the C-arm angle measurement results with built-in encoder and image-based angle measurement. The optical measurement system is used as ground truth information. The difference between one orientation estimation modality and ground truth is the orientation angle error of the tracking method. Errors in the three orientations were computed and collected in an error statistics overview. This overview allows an accuracy analysis for all systems and a direct comparison in between the different tracking modalities.

A one-time calibration procedure is performed. The C-arm is rotated into an initial position. In this position two measurements are recorded: the orientation data provided by the sensors (accelerometer, built-in encoder and image-based) and the ground truth orientation data. Afterwards the C-arm is rotated along one of its two axes with a predefined angle interval. In this second position sensor data and ground truth orientation data are recorded again. The records are taken for all orientations along the maximum rotation range of the C-arm at pre-defined intervals for both axes. A calibration function is constructed by polynomial fitting of the raw accelerometer angle measurements versus the ground truth angles. The calibrated angle values are computed by transforming the sensor-provided values by the calibration function. The calibration process is only needed once after the installation of the sensor.

C-arm orientation was measured in a repetitive multi-modality data acquisition experiment. The C-arm orientation was tracked for both rotation modes that are referred to as primary and secondary rotation angles. The rotation range was chosen to cover the operating distance of the C-arm during prostate brachytherapy procedure. The C-arm orientation was first measured with the optical measurement system. Subsequent to the recording of ground truth orientation a fluoroscopic image of the FTRAC fiducial was acquired. The X-ray images were post-processed after all data acquisition was completed to obtain orientation information. Next the accelerometer reading was recorded. The built-in encoder orientation value displayed on the C-arm screen was also recorded. Subsequently to data acquisition of the initial position, the C-arm was rotated to the next measurement position. All four orientation estimation modalities were carried out for 31 positions in the rotation range of a brachytherapy intervention. This was done for both primary and secondary rotation modes of the C-arm.
Results
The mean and standard deviation of the angle error were calculated for all tracking methods. This was done for primary angle rotation as well as for secondary angle rotation. The initial angle errors before calibration were compared with the angle errors after calibration. The results for primary angle rotations are shown in Table 1. The angle measurement error histograms, shown in Fig. 1, further illustrate the outcome of the calibration procedure applied to the tracking methods. The accuracy of orientation angle estimation with the accelerometer and the built-in encoders were both acceptable. Precision of the accelerometer-based angle estimation was much better compared to the built-in encoders, as demonstrated by the narrower histogram shape and lower standard deviation value. The FTRAC-based estimation method provided similar results as obtained by uncalibrated accelerometer and built-in encoder. However, compared to FTRAC the other methods had considerable better accuracy and precision after calibration.
Conclusion
The accelerometer proved to be able to provide sufficiently accurate C-arm orientation angle estimation for both rotation modes. Since an alignment of the accelerometer is laborious and subjective, we propose

Table 1 Mean angle errors for primary angle rotation of accelerometer, mechanical encoder and image-based orientation angle estimation

Primary angle rotation	Orientation angle error (initial)	Orientation angle error (after calibration)
Accelerometer	$1.3 \pm 0.1°$	$-0.1 \pm 0.0°$
Built-in encoder	$-0.2 \pm 0.3°$	$-0.1 \pm 0.2°$
FTRAC	$-0.1 \pm 1.3°$	N/A

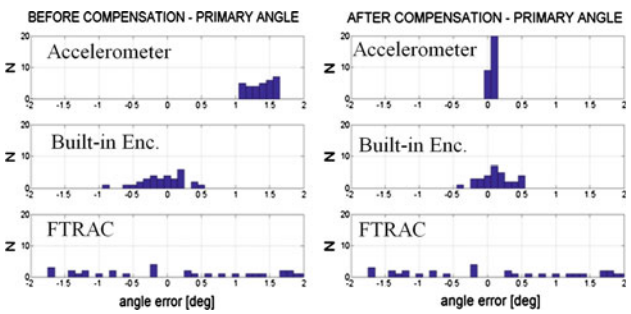

Fig. 1 Histograms showing the angle error distribution for primary angle rotation before calibration (*left*) and after (*right*), with accelerometer (*top row*), built-in encoder (*middle row*) and FTRAC (*bottom row*). The histogram bin size is 0.1°

and conducted a software-based calibration process that prevents user errors during setup. The built-in encoder angle estimation also showed accurate results regarding the C-arm's orientation recovery. The calibration process was able to further improve these results. FTRAC-based fluoroscope tracking did not deliver reproducible results in the orientation angle acquisition evaluation. The accelerometer-based orientation angle estimation is proved to be reliable and providing adequate accuracy and precision for prostate brachytherapy 3D seed reconstruction. In additional experiments the accelerometer demonstrated the ability to not only successfully measure the C-arm's orientation angle in the rotation range required for prostate brachytherapy seed position verification, but also confirmed that it is able to measure the C-arm's orientation angle in the full motion range of both rotation modes.

References

[1] Grzeda V, Fichtinger G (2010) C-arm rotation encoding with accelerometers. International Journal of Computer Assisted Radiology and Surgery 5:385–391

[2] Jain AK, Mustafa T, Zhou Y, Burdette C, Chirikjian GS, Fichtinger G (2005): FTRAC—a robust fluoroscope tracking fiducial, Medical physics 32(10):3185

[3] Lee J, Labat C, Jain AK, Song D, Burdette E, Fichtinger G, Prince J (2011) REDMAPS: Reduced-Dimensionality Matching for Prostate Brachytherapy Seed Reconstruction, IEEE Transactions on Medical Imaging 30(1):38–51

Development of MRI-compatible devices for real-time MR-guided orthopaedic surgery

F. Guettler[1,2], K. Winterwerber[3], C. Seebauer[2], J. Rump[2], A. Heinrich[1], M. De Bucourt[2], U. Teichgraeber[1]

[1]University Hospital Jena, Department of Radiology, Jena, Germany

[2]Charité—University Hospital, Department of Radiology, Berlin, Germany

[3]MGB Endoskopische Geraete GmbH, Berlin, Germany

Keywords Magnetic Resonance Imaging · MR Guided Procedures · Intraoperative Procedures · Surgical Instruments · Endoscopic Surgical Procedure

Purpose

Horizontally open-MRI with a magnetic field at 1 tesla allow good patient access and seamless intraoperative control under real-time image-guidance. This enables surgeons and interventionalists to introduce innovative approaches to complex MR-guided procedures i.e. orthopaedic surgery. For proof-of-concept of these methods various instruments and devices used in conventional orthopaedic surgery have to be developed MR-compatible. These are i.e. an air-driven bone-drilling system [1], a laparoscopic and endoscopic device, a pump and minimal-invasive instruments that can be used within the limited space of the MRI. In this work we present the results of the development and the application of the above mentioned instruments and devices in in vitro an ex vivo models i.e. at the human lumbar spine. The purpose of this work is to demonstrate a fully functional proof-of-concept environment including instruments and methods for real-time MR-guided abdominal or orthopaedic surgery for the methods of the MPLN [2], TEM and the drilling done i.e. for the osteoid-osteoma thermo-ablation [3] and retrograde drilling of osteochondral lesions of the talus [4] or bone biopsy.

Methods

To allow parallel real-time image acquisition using MRI and a laparoscope, a disposable MR-compatible endoscopic system was developed in the first step. An autoclavable MR-compatible laparoscopic device was developed, based on the knowledge derived from the endoscope. For the disposable prototype a micro LED and a video chip were installed on the tip of the instrument (see Fig. 1). The main body of the laparoscopic device was build from titanium

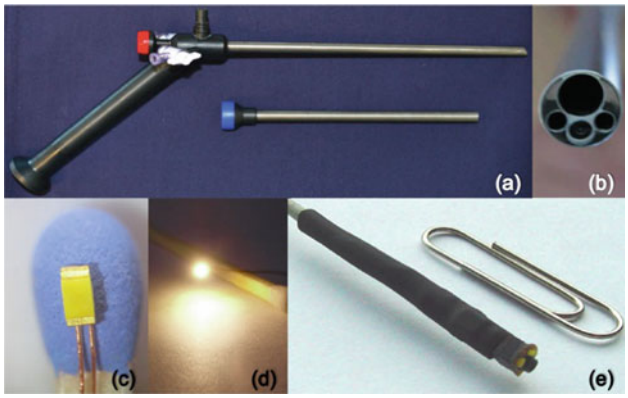

Fig. 1 MR-compatible laparoscopic device (*above*) with working-, suction- and irrigation-channel (*right*) and core electronic disposable MR-compatible endoscopic system (*below*) with multiple micro LED (*left*, *middle*)

and PEEK for pipes, shafts, sockets and heads as well as glass for the lenses and prism. The window is made from sapphire. Nickel is used for the sipes, shafts and brass is used for the sockets. A suction and irrigation channel, connected to an MR-compatible pump, were integrated beside the working channel. An MR-compatible camera and light source was mounted at the end of the device. MR-compatible laparoscopic instruments were also made by MR-compatible materials, mostly titanium with a special surface treatment. MR-compatible puncture needles, K-wires, dilators, micro scissors and forceps were made. According to ASTM standards, the MR-compatibility and the artefacts generated through the endoscopic system and laparoscopic device were determined for an open MRI (Panorama 1.0T HFO, Philips, Eindhoven, Netherlands). Experimental evaluation of the instruments was first done in a phantom model using human lumbar vertebral segments, imaged in an open MRI. Intervertebral discs ($n = 5$) were treated by using an interactive PDw TSE imaging. A butterfly coil (Philips, Eindhoven, Netherlands) for an optimal approach to the spine in prone position was used.

The construction of the MR-compatible bone drill (see Fig. 2 left) was realized according to feature and performance requirements derived from a commercially available non MR-compatible bone drill (Synthes Corp., Compact Air Drive II). Most of the components were newly planned and made of high-performance plastics and PEEK. A special designed, pneumatically controlled drive system of ferrite-free components was developed. An exchangeable attachment for the laying of the Kirschner wires was added. After prototype fabrication, the speed, weight, air consumption, operating pressure, perforation and noise level were measured and compared to commercially available systems. The torque and power of the drilling machine were determined experimentally.

According to ASTM standards, the MR-compatibility and the artefacts generated through the drilling machine were determined. Furthermore, an X-ray image was acquired to examine radio-density. The practical evaluation occurred under MR-navigation. During the phantom experiment ($n = 10$), the substantia compacta of a human corpse was drilled and a Kirschner wire was driven into compact bone. Furthermore, the autocalveability (at 134° C, 3 bar) was tested.

Results

The laparoscopic device and instruments required new methods for deformation, welding and stick of titanium alloys. The susceptibility artefact of titanium could be reduced with a special surface treatment. In the worst case the multifunctional device has a maximum artefact's size of $20.70 + -1.25$ mm (TSE) respectively $51.33 + -7.61$ mm (GE) according to ASTM F2119. The disposable endoscopic